

# THE EFFECT OF NONLINEARITY OF THE MATERIAL ON THE CONTACT PROFILES IN THE MANUFACTURE OF ARTIFICIAL JOINT

Haithem Hashem AL-Jawad  
University of Baghdad  
College of Engineering- Mech.Eng.Dept

## ABSTRACT:-

This research aims to induce the influence of nonlinear behavior material at mathematical structure by computer program for reducing the contact problem and stress state for the critical rounding profile of artificial joint. This subject computer must be modified to analysis the mechanism movement of the joint by taking different angle of rotation in the contact zone and at the edges of the joints.

For the contact problem with in nonlinear material, analytical solutions are obtained for both surface pressure and interior stress field. Cases of normal and frictional contact in both sliding and partial slip conditions are all treated.

The effect of the modification of the horizontal configuration on the stress distribution in rounded shapes of the joints have been analyzed experimentally using photo elastic pattern in different angles. The theoretical results have good agreement when compared with the experimental one.

## الخلاصة:-

أن فكرة البحث هو تقديم للسلوك اللاخطية للمواد في بناء رياضي بواسطة برامج الحاسوب للتقليل من مشاكل حالات التماس وحالة الإجهاد ذات التقوس الحرج للمفاصل الصناعية. موضوع الحاسوب هذا يجب أن يعدل لتحليل الحركة الميكانيكية للمفاصل بواسطة اخذ مختلف الزوايا للدوران في منطقة التلامس وعند حافات المفاصل. من اجل مشاكل التلامس مع المواد اللاخطية ، الحلول التحليلية يكون الحصول عليها لكلا سطح الانضغاطي ومنطقة دخول الاجهادات. حالات التلامس الطبيعي في كلا ظروف الانزلاق والانزلاق الجزئي جميعها تم معالجتها. أن تأثير التعديل في التشكيل الأفقي في توزيع الاجهادات في الأشكال الدائرية للمفاصل تحلل عملياً باستعمال نموذج للفوتو ايلاستك بزوايا مختلفة . النتائج النظرية جيدة مقارنة مع النتائج العملية.

Key words: Artificial Joint, Nonlinearity, contact profiles, slip contact.

## INTRODUCTION:-

It has been tried in the past to manufacture the artificial joint since 1861. The most important is the knee joint because the most of the weight of the human body is concentrated on this joint and the complicated of the shape in the contact zone between femoral bone and tibial bone especially in the moving case where the two bones are not in straight line. The design procedure of these contacts is usually one derived from experience, as it notorious ally difficult to determine the contact pressure in contrast to the hertzian contact where simple closed form solution exist. Here are some researches concerning the above outlined principles of nonlinearity of material contact: G.A. Ateshian [1994] describes the use of a stereophotogrammetry (SPG) system (Huiskes et al., 1985; Ateshian et al., 1991) for determining contact areas in diarthrodial joints, using a surface proximity concept similar to the one used by Scherrer et al. (1979).

This method consists of evaluating the proximity of the articular surfaces to determine joint contact areas using precise geometric models of the joint surfaces obtained from the SPG system, and precise kinematic data, also obtained from SPG. In this study, the SPG method for determining contact areas is compared to other commonly used methods such as dye staining, silicone rubber casting and Fuji film contact measurement techniques which have been often used and reported by other investigators.

M.P. Rosenwasser, and V.C. Mow[1999] Three-dimensional geometric models of the articular surfaces of the thumb carpometacarpal (CMC) joint were constructed using precise data obtained from stereophotogrammetry (SPG). It was demonstrated that by using a least-squares surface-fitting technique, the SPG data on the surface can accurately be described by a single parametric biquintic spline function. From this mathematical description, curvature maps of the surfaces were calculated for thirteen CMC joints (8 females, avg. 64 y.o.; 5 males, avg. 70 y.o.). The surface geometry of each joint was analyzed, comparisons were made between trapezoidal and metacarpal surfaces of the joint and differences determined between males and females. With regards to joint surface areas, the female trapezium is significantly smaller than that of the metacarpal. The shape of the female trapezoidal surface is also fundamentally different than that of males.

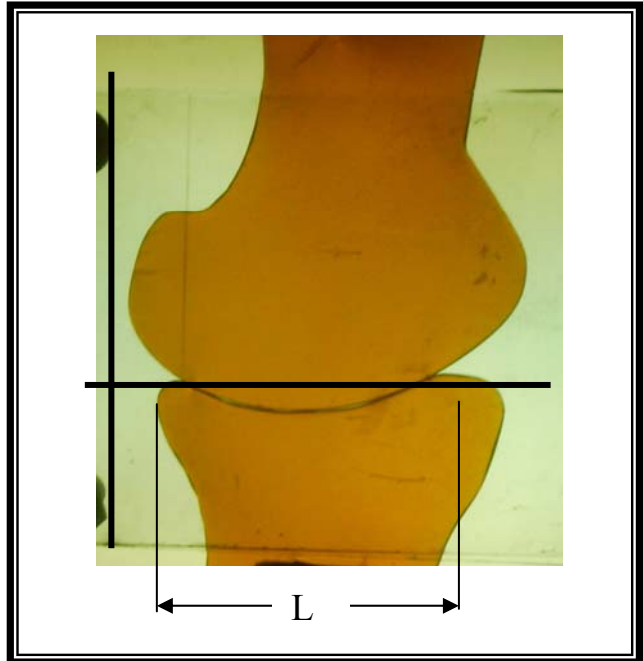
Cohen, Z.A., McCarthy[2000] This study assessed the three-dimensional accuracy of Magnetic Resonance Imaging (MRI) for measuring articular surface topographies and cartilage thicknesses of human cadaveric knee joints, by comparison with a calibrated stereophotogrammetric (SPG) method. Three-dimensional spoiled gradient recalled acquisition with fat suppression was employed with a linear extremity coil in a 1.5 T superconducting magnet and an imaging voxel size of 0.47 x 0.47 x 1.0 mm. For six cadaveric knees, the average accuracies of cartilage and subchondral bone surface measurements were found to be 0.22 mm and 0.14 mm respectively; the thickness measurements demonstrated an average accuracy of 0.31 mm. This study employed a manual and a semi-automated segmentation method for extracting topographic measurements from MRI; it was found that the much more efficient semi-automated method provided equally good and sometimes better accuracies than manual segmentation.

Dumitru I. Caruntu[2003] The objective of the present work is to determine the effects of the “thigh and calf” contact that occurs while the knee is maximally flexed, up to 165 degrees of knee flexion, on the loads transmitted across this joint. A two-dimensional anatomically based mathematical model of the human knee joint was used for this purpose. In this model, a single force was used to represent the resultant of the “thigh and calf” non-uniform contact stresses that act either on the tibia or the femur. Results were obtained to simulate isometric quad contractions associated with hamstrings co-contractions at a position of maximum knee flexion. Numerical calculations indicate that the predicted knee response differs greatly as you introduce the “thigh and calf” contact. This shows the importance of including this force when developing models that predict the response of the joint when it is maximally flexed.

For semi rounding contacts, the interfacial contact pressure is hypersensitive to small variations in surface geometry, particularly the presence of swarf near the two edges of the bone, however the corners are rounded off as shown in Fig.(1) .

Then most of these problems are complicated to nonlinear behavior which affects the shape and the stress distribution in the edges of the bone. The photo elastic pattern that used for experimental results and for different weights and angles of inclined shows good agreement with the purposed theoretical result.

Fig. (1) The geometry of the knee joint.



**THEORETICAL ANALYSIS:-**

**Normal Contact Laws:**

The general solution in the case of asymmetrical complete or incomplete contact over the  $-b \leq x \leq b$  range is given by Muskhelishvili's inverse of the singular integral equation as:

$$p(x) = -\frac{1}{\pi\sqrt{b^2-x^2}} * \left[ p - \frac{E^*}{2} \int_{-b}^b \frac{h(t)\sqrt{b^2-t^2}}{t-x} dt \right] \quad (1)$$

Where 
$$\frac{1}{E^*} = \frac{1}{E_1}(1-\nu_1^2) + \frac{1}{E_2}(1-\nu_2^2)$$

Have both  $p(b)$  and  $p(-b)$  are bounded (incomplete contact) and it may be proved that it must be true that  $p(\pm b) = 0$  which reduces the general solution for a contact over the range  $-b \leq x \leq b$  to

$$p(x) = \frac{E^*}{2\pi} \sqrt{b^2-x^2} \int_{-b}^b \frac{h(t)}{\sqrt{(b^2-t^2)(t-x)}} dt \quad \text{-----} \quad (2)$$

The applied load "p" is in equilibrium with the pressure distribution

$$) \quad p = - \int_{-b}^b p(x) dx = - \frac{E^*}{2} \int_{-b}^b \frac{h(t)t}{\sqrt{b^2 - t^2}} dt \quad \text{----- (3)}$$

Where 
$$h(x) = \begin{cases} -(a+x)/R & -b \leq x \leq a \\ 0 & -a \leq x \leq +a \\ -(x-a)/R & +a \leq x \leq b \end{cases}$$

**Partial Slip Contact:**

When the load "p" applied normal to the contact zone then the pressure distribution under such conditions has been found.

If the loading "p" is applied at inclined support to the contact zone with angle (α) with the vertical axis.

Then the two component of the load is normal contact load which is take the hertzian contact and tan genial component (Q) which causes sliding and slip contact and can be found by the equation:-

$$Q = \int_L q(\lambda) d\lambda \quad \text{----- (4)}$$

Where q (λ) can be found from the equation which relates the displacement of particles parallel with the surface to the surface traction

$$\frac{E^*}{2} g'(x) = \frac{1}{\pi} \int_L \frac{q(\lambda)}{x - \lambda} d\lambda + \beta p(\lambda) \quad \text{----- (5)}$$

Where  $g'(x) = dg(x)/dx$ ,  $g(x)$  is the relative tangential displacement of surface particles.

**GENERAL NONLINEAR SOLUTION:-**

Along the contact region in the joint there are different radiuses of curvatures which will causes different pressure distribution at any point since the pressure dependence on the shape of the two contact bodies.

This can be represented by a nonlinear form written by:

$$N(w) - p = 0 \quad \text{----- (6)}$$

Where N: is any nonlinear differentiable operator

(w): is a function or set of function satisfying prescribed linear initial boundary conditions.

P: is a known function or set of known function.

The governing equations of the general nonlinear continuum problem in the presence of small displacements and strains, i.e. equilibrium, compatibility, direct and inverse constitutive law are:

$$\sigma_{ij,j} + \bar{F}_i = 0$$

$$\begin{aligned} \sigma_{ij} n_j &= \bar{p}_i \\ \epsilon_{ij} &= \frac{i}{2}(u_{i,j} + u_{j,i}) \\ u_i &= \bar{u}_i \\ \sigma_{ij} &= \psi(\epsilon_{ij}) \\ \epsilon_{ij} &= \phi(\sigma_{ij}) \end{aligned}$$

Where  $(\psi)$  and  $(\phi)$  are differential or integral or generally nonlinear operators

$$\left( \frac{\partial}{\partial x_j} \right) = d \frac{(\quad)}{d x_j}$$

$n_j$  are the components of the outward normal unit vector.

$\bar{F}_i(t)$  are the volume forces which acted externally.

$\bar{u}_i(t)$  prescribed displacement.

$\bar{P}_i(t)$  are the surface forces per unite length.

$$\begin{aligned} \sigma_{ij}(x,t), \epsilon_{ij}(x,t) \\ u_i(x,t) \end{aligned}$$

The stresses, strains and displacements space time functions and are to be determined by iteration method using a NLSYST program which solves the nonlinear system. Some judgment is needed to use NLSYST, first the initial guesses for values of the variables must be near to a solution to give convergence, second the value for delta should be small enough to give a reasonable approximation to the partial derivative but not so small as to lead to excessive round-off.

**EXPERIMENTAL ANALYSIS:-**

The experimental method used is photo elasticity and the profile and external dimension of the joint is all exactly 2½ times the size of the external of facilitate handling and data collection.

This model was a two dimensional representation of a three –dimensional structure, with the profiles bring taken in the axial radial plane of the three dimensional component.

As the loading required for these models was purely axial no special loading frame was required.

In photo elasticity the value of the stresses can be found by the equation:

$$\sigma_1 - \sigma_2 = \frac{CN}{t} \text{----- (7)}$$

Where  $\sigma_1, \sigma_2$  are the principle stresses

$$C = \lambda/k$$

$\lambda$  Is the wave length

K =is the relative stress-optic coefficient which is a material property.

N is the fringe number.

T is the thickness of the specimen

We could write eq. (7) as: 
$$\frac{P}{N} = CW$$

Where p is the applied force

W is the width of the specimen

The fringe pattern can be shown in Fig.(1) for different loads.

The properties of the photo elastic material is given by the material are CR-39 which has:

value of the fringe order	passions ratio	young modulus	tensile strength
C=100Ib/in.	$\nu=0.42$	300000 Ib/in	3000Ib/in

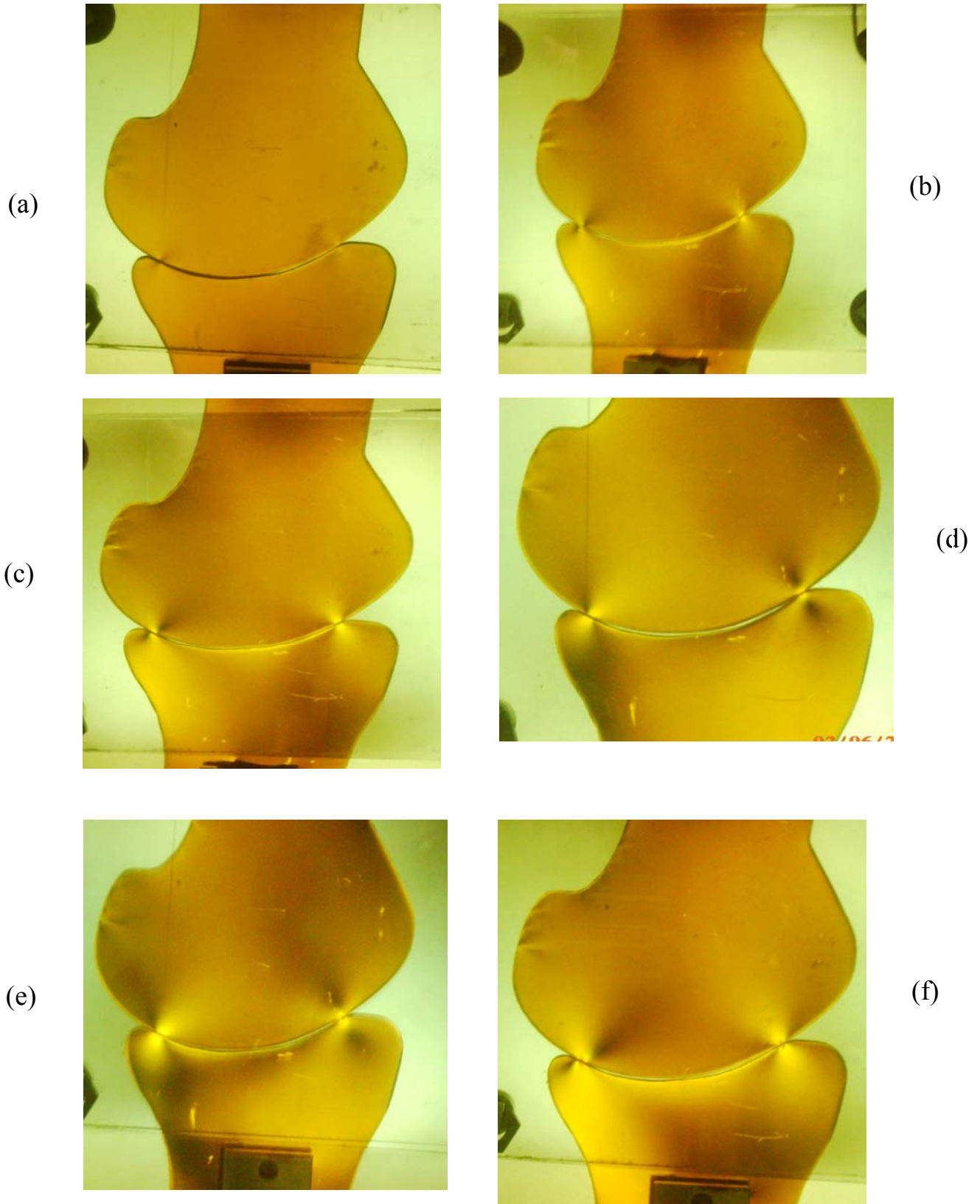


**Fig. (2) The pattern of the knee joint in angle = 0 at the various load (a).5kg (b)1kg (c)1.5kg (d)2kg (e)2.5kg (f)3kg**

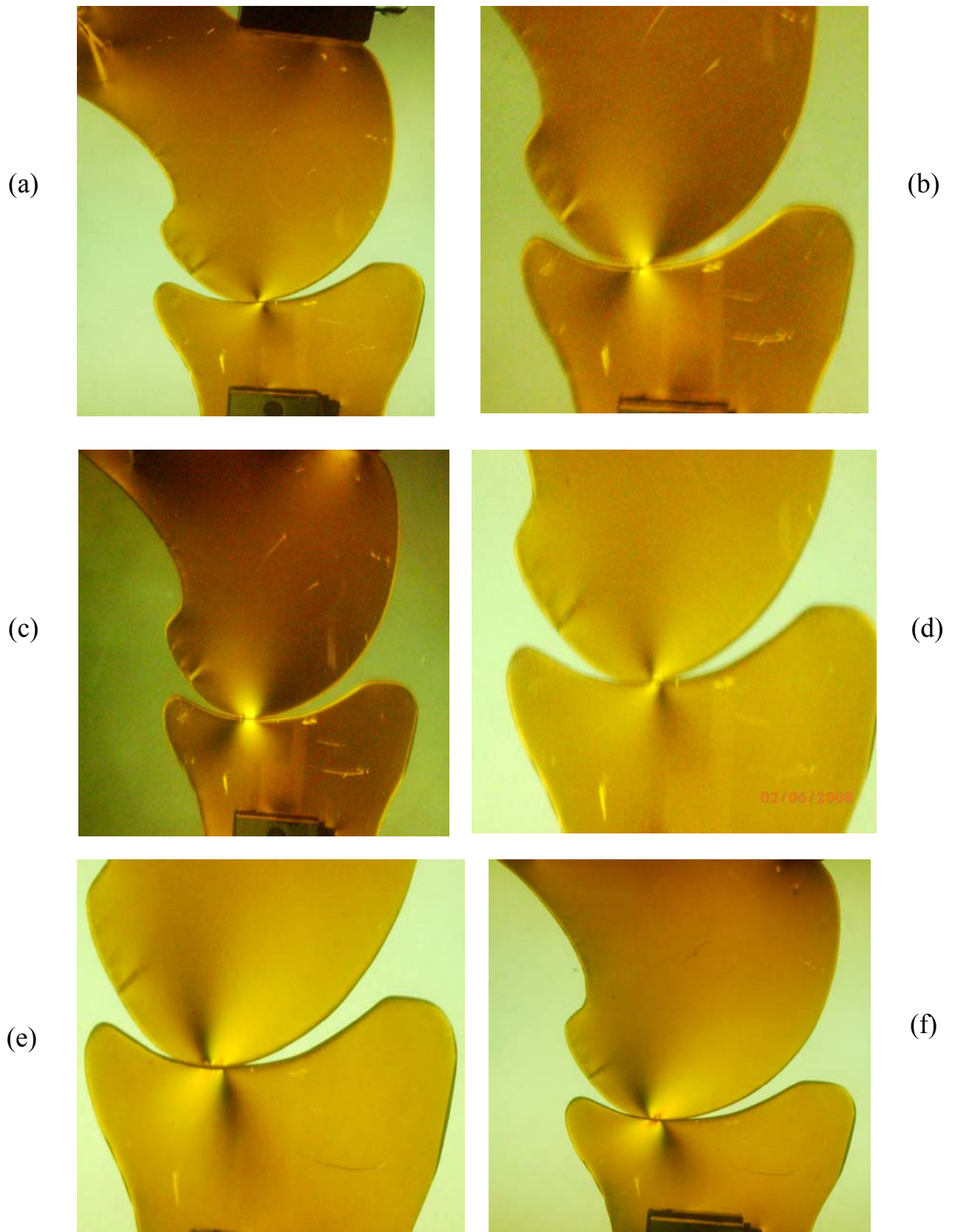


**Fig. (3) The pattern of the knee joint in angle =30 at the various load  
(a).5kg (b)1kg (c)1.5kg (d)2kg (e)2.5kg (f)3kg**

**RESULTS:-**

The results that obtained from the linear values of each point along the contact surfaces are computed by non –linear interpolation of all points in the compatibility and equilibrium equations shown in the theoretical analysis.

As shown in Fig. (4) the variation of the axial strain along the non dimensional contact line  $X/L$  (where  $l$  is the length of contact surfaces.) This analysis was done for linear relation of the normal contact pressure at every point in the contact region .While when using the analysis of transformation to non linear interpolation it gives a different result which is greater than the linear one.

In Fig.(5) the effect of sliding contact along the contact line shows that at the first points of the contact length have low values and then increased at the end point which is mean that there is two supported points having high value and must be taken into consideration.

This phenomena have been cleared when we are looked at Fig.(6) which shows the variation of normal and sliding contact stresses along the contact length and the maximum stresses obtained at these two points

While increasing the load applied from 30 Kg to 80 Kg then the variation of strains and compind stresses in figures (7), (8) and (9) shows that the values of strain and contact stresses are increased and the two points that supports the applied load have been shifted to the first and end edges and this is because of high effect of sliding contact load on the position of the maximum contact load.

In figures (10), (11), (12), (13), (14), and (15) the variation of strain and stresses along the contact length have been affected by changing the applied load with angle  $\alpha=30$  which is max inclination taken into consideration with the principle axis.

Since the applied load will be analyzed to vertical and horizontal components and the shear sliding strain and stress have very high effect on the contact length and the position of the two supported point's .Also this behavior will be changed with increasing the applied load.

To support our results we have done some experimental prototype specimen of photo elastic material and applied the equivalent loads of 30 Kg and 80 Kg which gives as shown in Fig.(16) and (17) .The experimental results shown that some points have values which is nearest to the linear values at normal load of 30 Kg while when the loading increased the values of the combined stresses will be nearest to the non linear values and the behavior will be more complicated because the sliding contact stress have been increased and the contact length especially we could see it when the applied load inclined with angle  $\alpha=30$  .

**CONCLUSION:-**

The contact stresses in artificial joint are very complicated since the shape of the contact zone will be flacuted from simple linear behavior to non linear compatibility and equilibrium equations which dependent on the values of hertzian contact stress at any point along the contact length.

This behavior will effect on the shape of the joint and on the stress distribution especially near the edges of contact zone. This effect has pronounced widely when the applied load inclined with the principle axis and that is agreement with the experimental results.

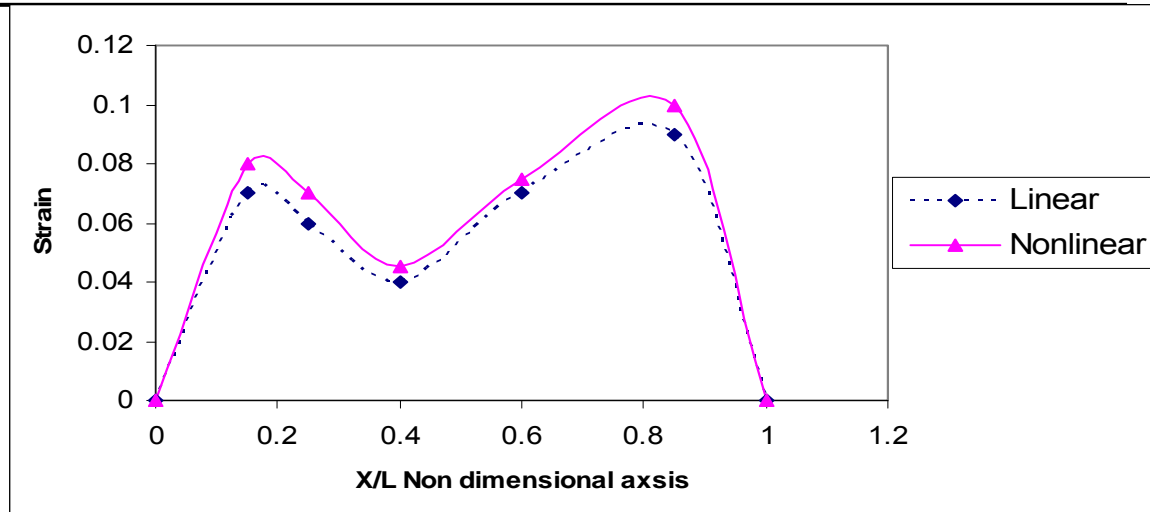


Fig (4) The variation of the theoretical axial strain along the contact line under 30Kg

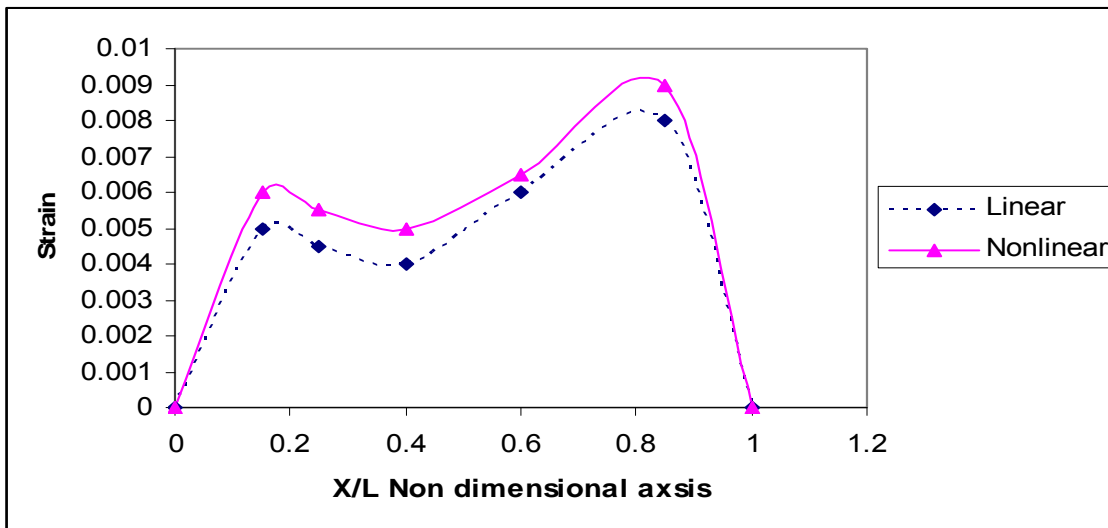


Fig (5) the value of the theoretical sliding strain along the contact line under 30 Kg

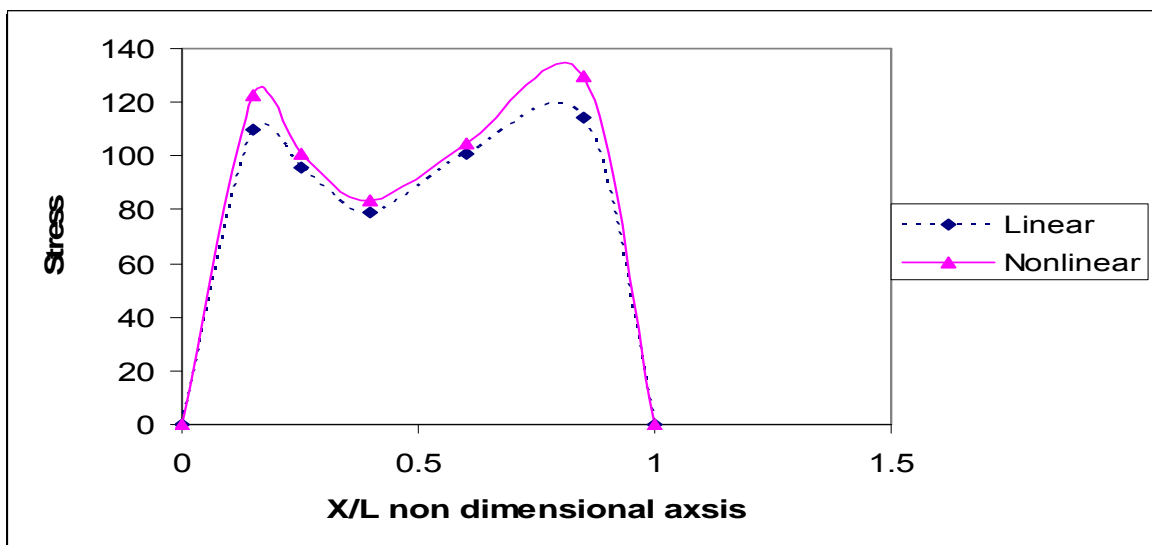
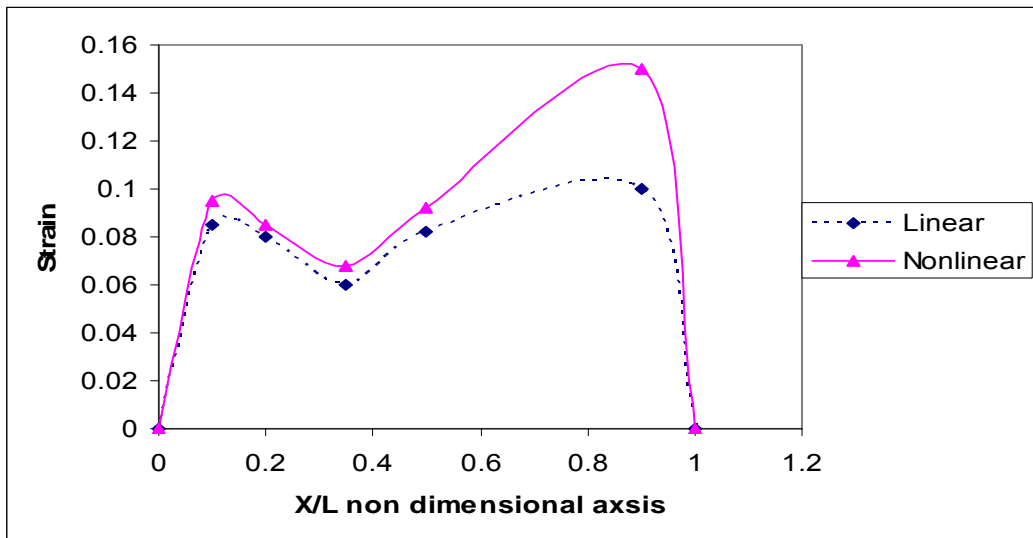
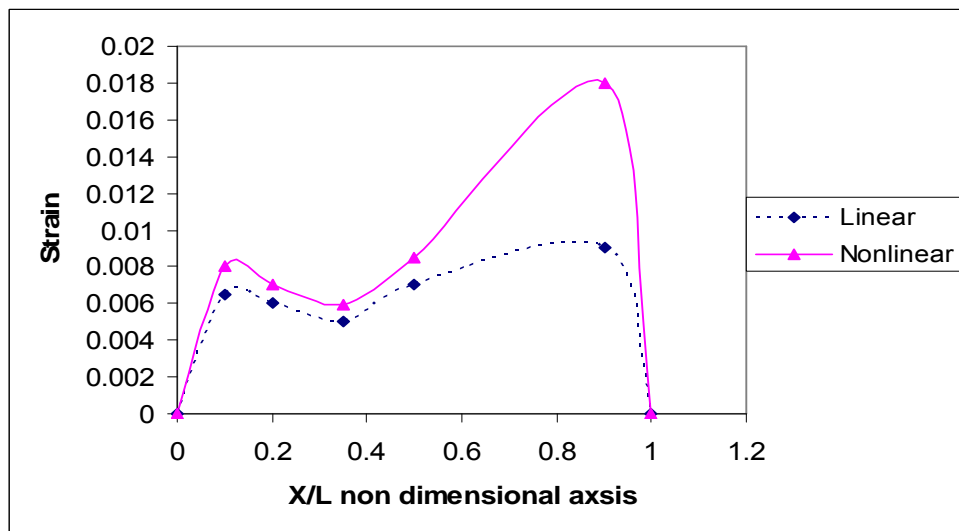


Fig. (6) The variation of the combined normal and sliding stresses along the contact line under 30 Kg



**Fig. (7) The variation of the theoretical axial strain along the contact line under 80 Kg**



**Fig. (8) The variation of the theoretical sliding strain along the contact line under 80 Kg**

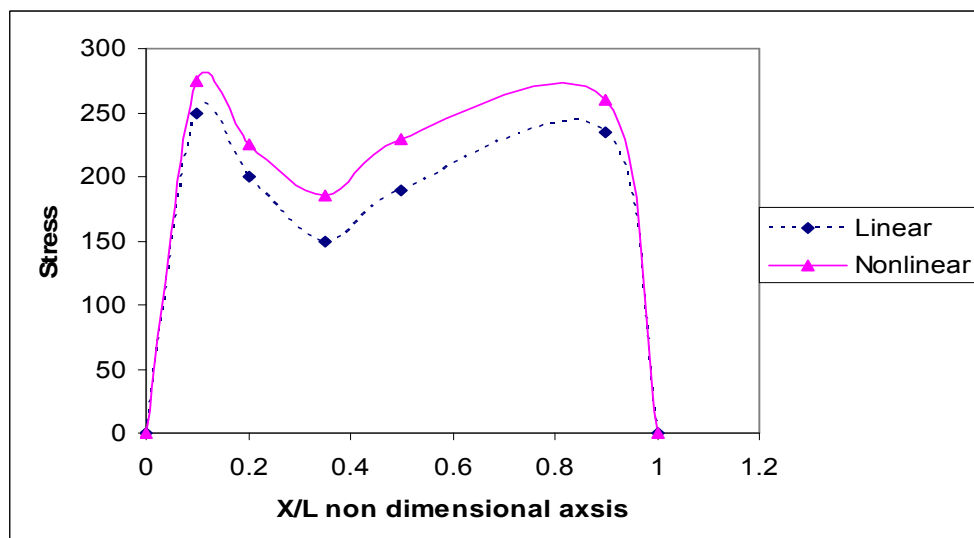


**Fig. (9) The variation of the combined normal and sliding stresses along the contact line under 80 Kg**

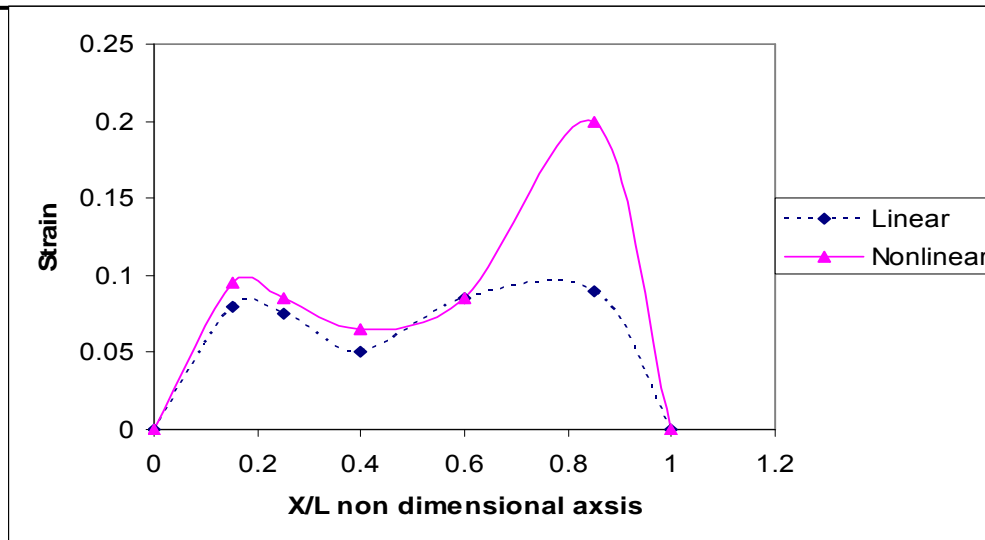


Fig. (10) The variation of the theoretical axial strain along the contact line under 30 Kg with inclined angle  $\alpha = 30^\circ$

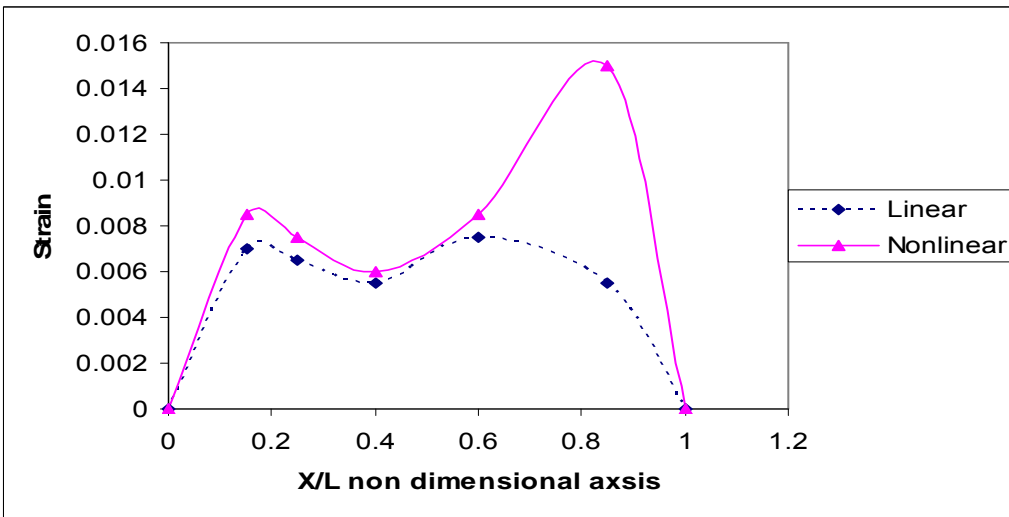


Fig. (11) The variation of the theoretical sliding strain along the contact line under 30 Kg with inclined angle  $\alpha = 30^\circ$

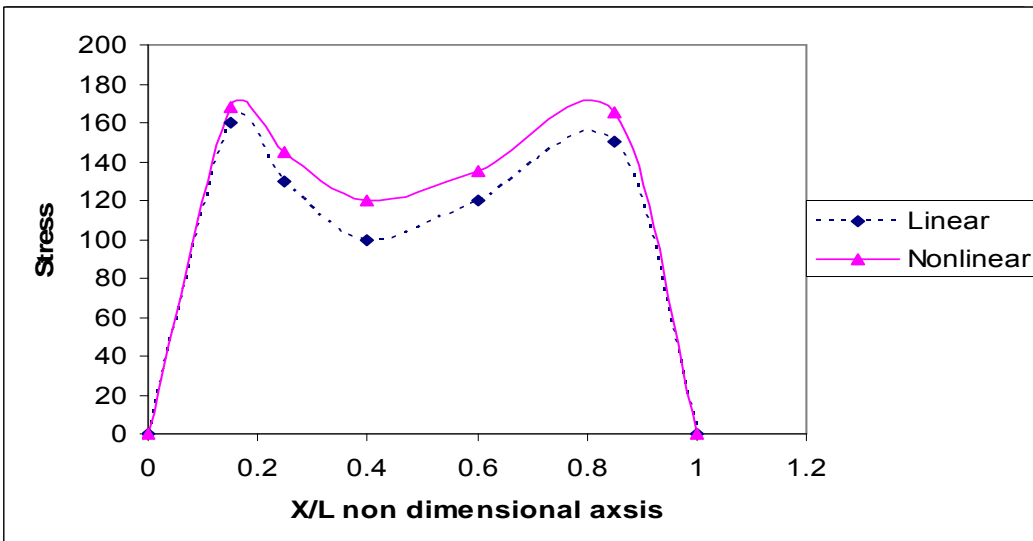


Fig. (12) The variation of the combined normal and sliding stresses along the contact line under 30 Kg with inclined angle  $\alpha = 30^\circ$

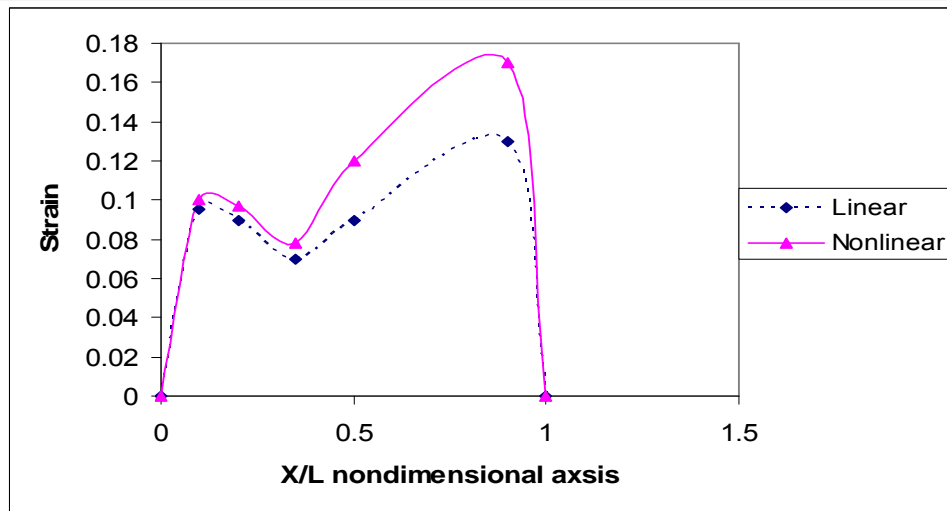


Fig. (13) The variation of the theoretical axial strain along the contact line under 80 Kg. with inclined angle

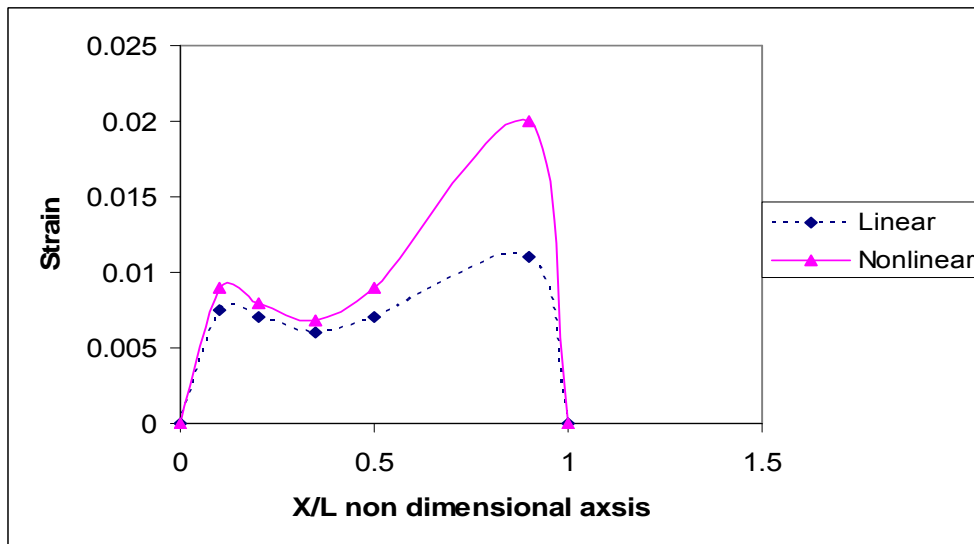


Fig. (14) The variation of the theoretical sliding strain along the contact line under 80 Kg. with inclined angle  $\alpha$

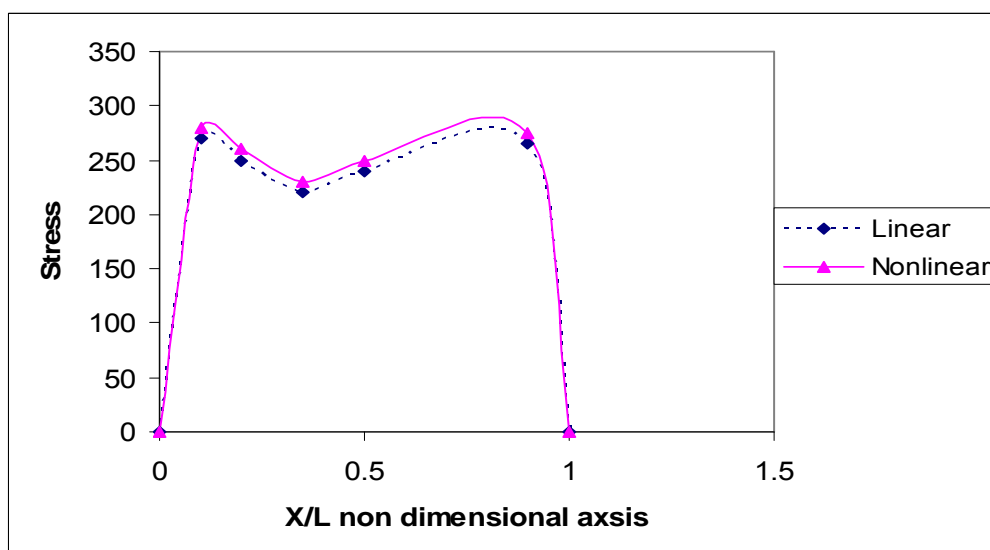


Fig (15) The variation of the combined normal and sliding stresses along the contact line under 80 Kg. with inclined angle  $\alpha = 30^\circ$

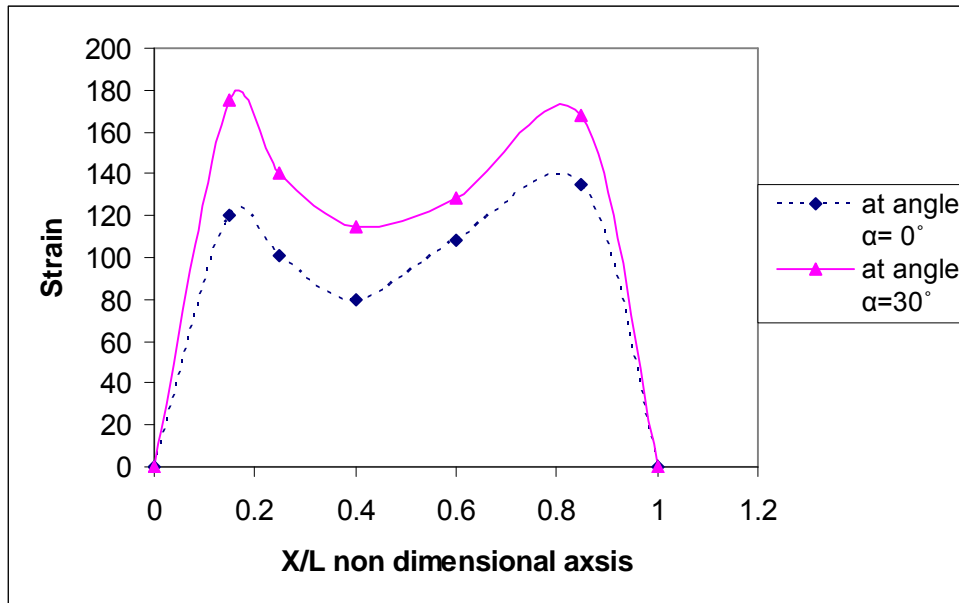


Fig. (16) The compares ion between the experimental results for 30 kg with angle  $\alpha = 0^\circ$  and  $\alpha = 30^\circ$

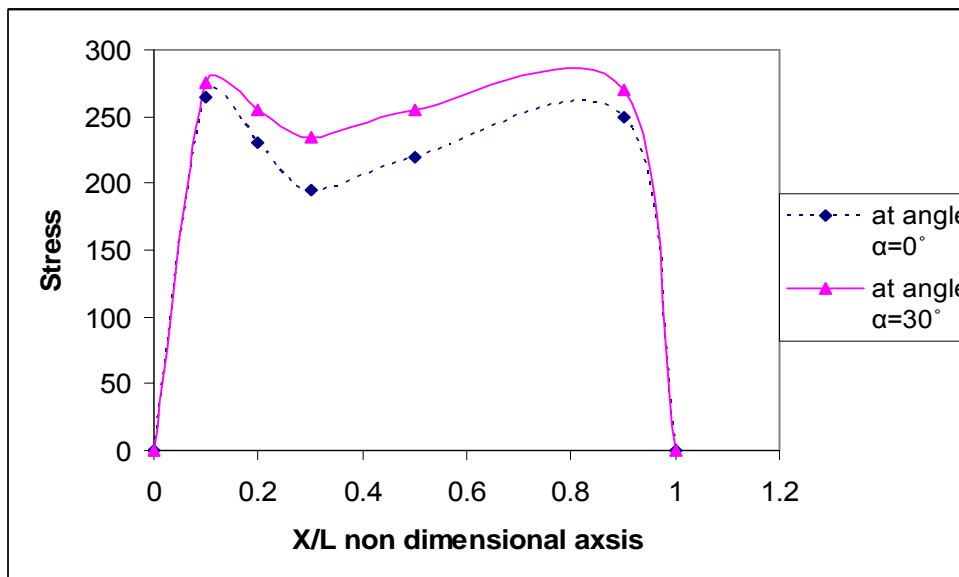


Fig. (17) The compares ion between the experimental results of 80 kg with angle  $\alpha = 0^\circ$  and  $\alpha = 30^\circ$

Symbol	Noun
P	Load or applied force
N	Nonlinear differentiable operator
P	Known function or set of known function
w	Function or set of function satisfying prescribed linear initial boundary conditions
$\Psi, \varphi$	Differential or integral or generally nonlinear operators
	The components of the outward normal unit vector
$(t)$	The volume forces which acted externally
$(t)$	Prescribed displacement
$(t)$	The surface forces per unite length
$\sigma_1, \sigma_2$	The principle stresses
$\lambda$	The wave length
K	The relative stress-optic coefficient which is a material property
N	The fringe number
T	The thickness of the specimen
W	The width of the specimen

**SYMBOLS:-** $n_j$  $\bar{F}_i$  $u_i$  $p_i$ **REFERENCES:-**

A 1Ateshian, G.A., Kwak, S.D., Soslowsky, L.J., and Mow, V.C. (1994) stereophotogrammetric method for determining in situ contact areas in diarthrodial joints, and a comparison with other methods. Journal of Biomechanics, 27:111-124.

Cohen, Z.A., McCarthy, D.M., Kwak, S.D., Legrand, P., Fogarasi, F., Ciaccio, E.J., and Ateshian, G.A. (2000) Knee cartilage topography, thickness, and contact areas from MRI: In vitro calibration and in vivo measurements. Osteoarthritis and Cartilage, 7:95-109

---

Dumitru I. Carun Mohamed Samir Hefzy Vijay K. Goel Henry I. Goitz Michael J. (2003)

Dennis Modeling the knee joint in deep flexion “thigh and calf” contact Summer Bioengineering Conference, June 25-29, Sonesta Beach Resort in Key Biscayne, Florida

Hung, C.T.(2004) Functional Properties of Native Articular Cartilage. In: Functional Tissue Engineering: The Role of Biomechanics. F. Guilak, D. Butler, S.A. Goldstein, D. Mooney (eds), Springer-Verlag, New York, pp.46-68.

Mow, V.C., and Ateshian, G.A. (1997) Friction, Lubrication, and Wear of Diarthrodial Joints. In: *Basic Orthopaedic Biomechanics*, V.C. Mow and W.C. Hayes (eds), Raven Press, New York, 2nd ed, pp. 275-315.

Mow, V.C. and Flatow, E.L. (2000) Biomechanics. In: Orthopaedic Basic Science, J. A. Buckwalter, T.A. Einhorn, and S.R. Simon (eds), American Academy of Orthopaedic Surgeons, Rosemont, IL, 2nd ed, pp. 133-180.

Rosenwasser, M.P., and Mow, V.C. (1992) Curvature characteristics and congruence of the thumb carpometacarpal joint: Differences between male and female joints. *Journal of Biomechanics*, 25:591-607.

Wang, X. (2000) Boundary Conditions at the Viscous Sliding Interface of Incompressible Porous Deformable Media. In: *Multifield Problems, State of the Art*. A.-M. S ndig, W. Schiehlen, W. Wendland (eds), Springer Verlag, Berlin, pp. 115-124.